MORPHOLOGY OF ULTRAFINE COBALT AND NICKEL POWDERS

A.S. Kurlov[1], A.I. Gusev[1] and A.A. Rempel[1,2]

[1]Institute of Solid State Chemistry, Ural Division of the RAS, Ekaterinburg 620990, Russia
[2]Ural Federal University named after First President of Russia B.N. Yeltsin, Ekaterinburg 620002, Russia

Abstract. The phase composition, particle size distribution and morphology of cobalt and nickel powders and foam nickel are examined by X-ray diffraction, laser diffraction and scanning electron microscopy methods. Cobalt and nickel powders obtained by electrolysis of solutions are found to have a dendritic structure. It is shown that the morphology and microstructure of particles of nanostructured cobalt and nickel powders and of nanostructured foam nickel can be described with a three-level (according to particle size) model.

1. INTRODUCTION

Cobalt and nickel powders are used in powder metallurgy as components of metal-cutting and drilling hardmetals, in the production of magnets, accumulators, filter elements, electric contacts, specialized coatings, coloring agents, catalysts, welding rods, composite adhesives, ferrites, and conducting rubber. The prospects of application of ultra-dispersed and especially of nanocrystalline nickel and cobalt powders in different areas are constantly expanding. Nanosized cobalt powders have high saturation induction and are promising materials for production of data recording and storage systems, magnetic fluids, nanostructured composite materials and also find application in magnetic resonance tomography [1-3]. Magnetic nanoparticles of cobalt and nickel can be used for targeted transfer of biologically active and pharmaceutical substances in biology and medicine [2-4]. Suspensions of Ni and Co are employed as oil additives for in-process restoration of worn-out parts of automobile and other engines [5]. One of the developing industries is the production of chemical current sources using cobalt and nickel nanopowders and nanostructured

foam nickel [6-8]. In November 2011, a group of researchers [9] has produced a superlight and durable nanostructured nickel-based material, which resembles foam nickel, but has an ordered structure. This material is a three-dimensional cage of hollow nickel tubes with ~100 nm thick walls. Similar to foam nickel, it can find application as a light electrode in chemical current sources to increase their capacity and reduce weight, as well as a catalyst carrier with a large surface area.

2. EXPERIMENTAL

Two fine-grained cobalt powders were used in this study. Thermochemical powder Co(th) was obtained by a one-step thermochemical method of decomposition and reduction of cobalt carbonate $CoCO_3$ in hydrogen atmosphere at temperature up to 620 °C. Electrolytic powder Co(el) was produced by electrochemical deposition from an aqueous solution of cobalt sulfates and ammonium, in which ground plates of metallic cobalt were an additional source of Co^{2+} ions.

Fine-grained nickel powders Ni(cb) and Ni(el) were synthesized by carbonyl and electrochemical

---

Corresponding author: A.S. Kurlov, e-mail: kurlov@ihim.uran.ru

methods, respectively. The carbonyl powder Ni(cb) was obtained by decomposition of nickel carbonyl $Ni(CO)_4$ in a gas-vapor mixture containing not more than 1 vol.% of oxygen under pressure 1 atm at temperature ~200 °C, and the electrolytic powder Ni(el) was produced by electrolysis of ammonia solution of nickel sulfate where nickel anode was an additional source of Ni^{2+} ions.

To produce foam nickel, metallic nickel was deposited from the carbonyl gaseous phase on open-cell foamed polyurethane. Then the nickel-coated matrix was annealed to remove the organic polymer carrier.

The phase composition of Co and Ni powders and of foam nickel was examined by X-ray diffraction (XRD) method in the angular range $2\theta = 10\text{-}140°$ with a step 0.03° and scanning time at point 2 sec on a Shimadzu XRD-7000 diffractometer in Cu$K\alpha_{1,2}$ radiation. In addition, from the broadening of XRD reflections we determined the average size of coherent-scattering regions (CSR), which can be considered in the first approximation as the average size $<D>$ of powder and foam nickel nanoparticles. The diffraction reflection profiles were modeled with the pseudo-Voigt function, and the background was described by the polynomial functions.

Diffraction reflection broadening $\beta(2\theta)$ was determined as $[(\text{FWHM}_{exp})^2 - (\text{FWHM}_R)^2)]^{1/2}$, where FWHM_{exp} is the full width of the reflection at half maximum (height) of the experimental reflection and FWHM_R is the diffractometer resolution function. The diffractometer resolution function FWHM_R was found in a special diffraction experiment with a standard reference sample of cubic lanthanum hexaboride LaB_6 (NIST Standart Reference Powder 660a) having a tabulated lattice constant $a = 0.41569162$ nm. The resolution function of a Shimadzu XRD-7000 diffractometer has the form $\text{FWHM}_R(2\theta) = (u\tan^2\theta + n\tan\theta + w)^{1/2}$, where $u = 0.0061$, $\nu = -0.0046$, and $w = 0.0078$.

For nanostructured materials, the broadening as a rule is caused by both the small size of particles and the microstrains. Broadening due to the small size D of particles or grains is named size broadening and broadening caused by the lattice microstrains is named strain broadening. In order to separate these contributions to the experimental reflection broadening, the extrapolation Williamson-Hall method [10-14] is used. It is based on the construction of the dependence of the reduced broadening $\beta^*(2\theta)=[\beta(2\theta)\cos\theta]/\lambda$ of the (*hkl*) diffraction reflection on the scattering vector length $s = (2\sin\theta)/\lambda$. The average size of CSR assumed as the average size $<D>$ of nanoparticles was determined by extrapolating the dependence of the reduced broadening $\beta^*(2\theta)$ on the scattering vector s to the value $s = 0$.

The particle size distributions in the Co and Ni powders were determined using a HORIBA LA-950V2.

The spectral analysis of the powders was performed on a Perkin Elmer SCIEX-ELAN 9000 mass-spectrometer. According to the spectral analysis data, the content of impurity elements in the cobalt powders was not greater than 0.05 wt.% of Fe and Ni and 0.02 wt.% of Si, C, and Cu. In the nickel powders, the content of impurity elements did not exceed 0.01 wt.% of Fe and Co and 0.01 wt.% of Si and Cu. The content of other impurity metals in the examined cobalt and nickel powders was maximum 0.005 wt.%.

The morphology of nickel and cobalt powders and foam nickel was studied by the high resolution scanning electron microscopy (HRSEM) method on electron microscopes JEOL JSM 6390 LA and Zeiss NEON 40 EsB.

3. RESULTS AND DISCUSSION

3.1. Cobalt powders

Scanning electron microscopy of thermochemical powder Co(th) was carried out with 1000 to 50000× magnification. At a magnification of 10000 times, it is seen that extended particles ~1 μm in length and ~0.5 μm in width are not bound with each other and form no dendritic microstructures (Fig. 1). SEM studies showed that the Co(th) powder is bimodal judging by the size and shape of its particles. This is especially well seen at 50000× magnification (Fig. 1c): along with large 0.5 to 1.0 mm particles, the powder contains extended 150 to 250 nm long and ~100 nm wide particles, which are aggregates of nanoparticles smaller than 100 nm. In a diffraction experiment, the presence of small particles should result in broadening of diffraction reflections.

Fig. 2 demonstrates XRD patterns of Co(th) and Co(el) powders. As is seen, both powders are two-phase. According to quantitative X-ray phase analysis, the thermochemical powder Co(th) contains ~22 wt.% of the low-temperature hexagonal (space group $P6_3/mmc$) phase α-Co with the lattice constants $a = 0.25088\pm0.00006$ nm and $c = 0.40762\pm0.00022$ nm and ~78 wt.% of the high-temperature cubic (space group $Fm\overline{3}m$) phase β-Co with the lattice constant $a = 0.35448\pm0.00001$ nm. The electrochemical powder Co(el) (Fig. 2b) contains ~52 wt.% of hexagonal α-Co and ~48 wt.% of cubic β-Co. Analysis of the diffraction reflection
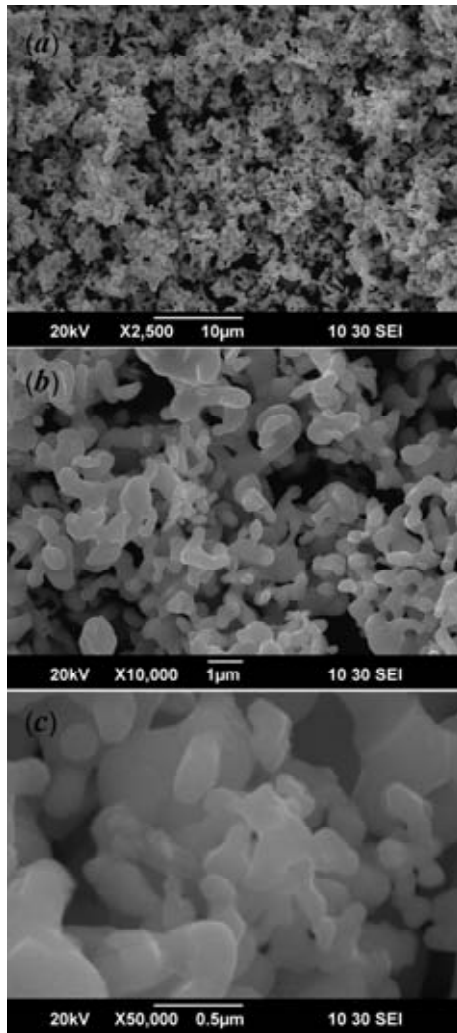
Fig. 1. Scanning electron microscopy of thermochemical cobalt powder Co(th): (a) 2500×, (b) 10000×, and (c) 50000× magnification.

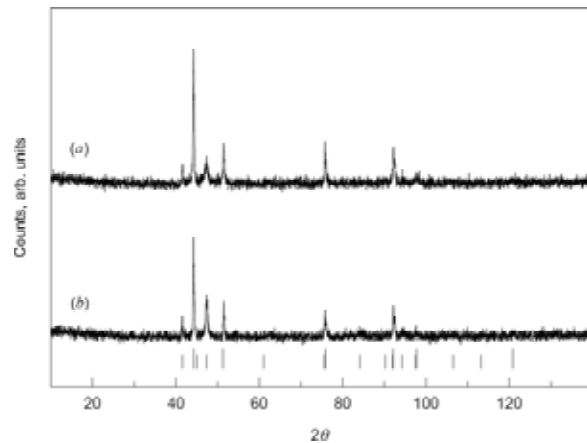**Fig. 2.** XRD patterns of (a) thermochemical Co(th) and (b) electrolytic Co(el) cobalt powders recorded in $CuK\alpha_{1,2}$ radiation. Both powders are two-phase and contain a cubic (space group $Fm\overline{3}m$) phase β-Co and a hexagonal (space group $P6_3/mmc$) phase α-Co. Long and short ticks correspond to diffraction reflections of the cubic β-Co and hexagonal α-Co cobalt phases, respectively.

profiles showed that in both powders the reflections of cubic as well as of hexagonal cobalt are broadened. From diffraction reflection broadening we determined the average size of the CSR for the cubic phase β-Co, which was 40±10 nm for the Co(th) powder and 50±10 nm for the Co(el) powder. The size of particles of the hexagonal phase α-Co in the examined cobalt powders could not be estimated by means of the XRD method because of a small number of observed reflections. Nevertheless, the large broadening of diffraction reflections for the hexagonal phase suggests that the CSR of this phase should not be greater than 50 nm. Sintering of WC-Co hardmetals with 4 to 16 wt.% of cobalt is carried out at a temperature above 1000 °C [15,16], which is much higher than the temperature of the phase transition α-Co ↔ β-Co, 427 °C. Therefore the two-phase character of the cobalt powders used as a metallic binder does not affect the structure

and properties of produced WC-Co hardmetals since already at the initial stages of sintering cobalt becomes single-phase and contains only cubic β-Co [16-18].

According to the particle size distributions, the average particle size is equal to 22 and 23 μm for the Co(th) and Co(el) powders, respectively (Fig. 3). The smallest particles in the Co(th) powder are ~2.4 μm in size and half of all the particles are less than 12.5 μm in size. The peculiarity of Co(th) powder is almost bimodal particle size distribution with a pronounced maximum for $D = 12$ μm and a weak peak for $D \approx 60$ μm (Fig. 3). The smallest particles in the Co(el) powder are ~2.5 μm in size, half of all the particles are less than 20 μm in size, and 95% of all the particles have a size no more 45 μm. Thus, analysis of laser diffraction data shows that the particles of both powders are highly agglomerated.

Comparison of XRD (Fig. 2a) and SEM results (Fig. 1) reveals that the cubic phase b-Co in the Co(th) powder is present mainly as nanocrystalline particles of average size 40 nm. The nanoparticles of the both phases make up extended 300 to 2000 nm long and ~100 nm wide aggregate particles. It is seen from Fig. 1a that the particles of thermochemical Co(th) powder are combined into a branched agglomerates of size 10-20 μm. This is in accordance with the data on the particle size distribution (Fig. 3).

SEM studies of the electrolytic powder Co(el) at 1500× magnification showed that its particles are 2 to 5 μm in length and about 1 μm in width and form
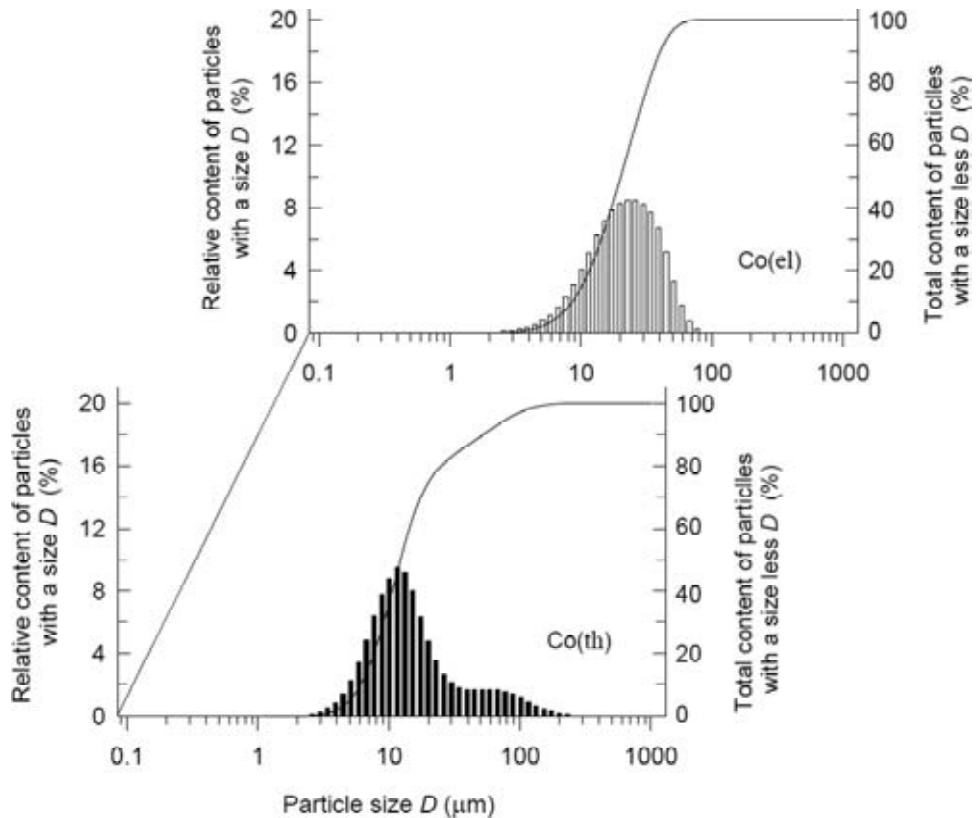
Fig. 3. Particle size distribution in the thermochemical Co(th) and electrolytic Co(el) cobalt powders. The distribution is determined by the laser diffraction method on a HORIBA-Laser LA-920 Analyzer.
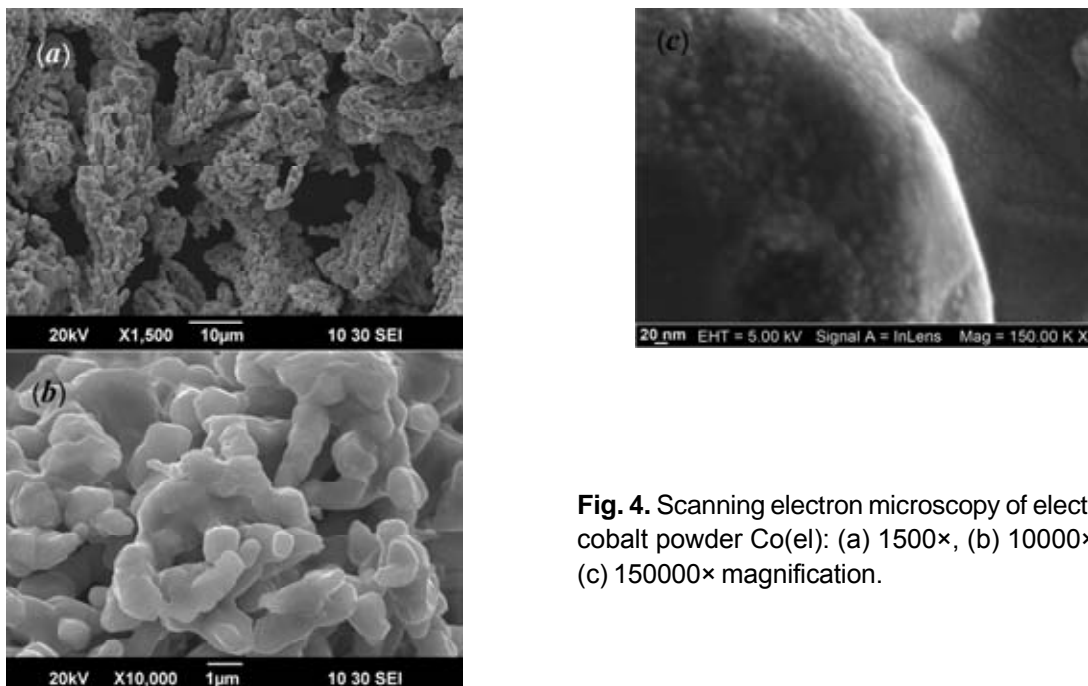

Fig. 4. Scanning electron microscopy of electrolytic cobalt powder Co(el): (a) 1500×, (b) 10000×, and (c) 150000× magnification.

a branched dendritic structure (Fig. 4a). Dendrites have a size of ~10×20 μm, which coincides with the results of particle size distribution (Fig. 3). At a magnification of 10000 times it becomes clear that the large particles are aggregates of smaller par-

ticles having comparable (~1 μm) dimensions in all directions (Fig. 4b), the microstructure of the Co(el) powder being monomodal. This is in complete agreement with the data on the particle size distribution in the Co(el) powder (see Fig. 3). The
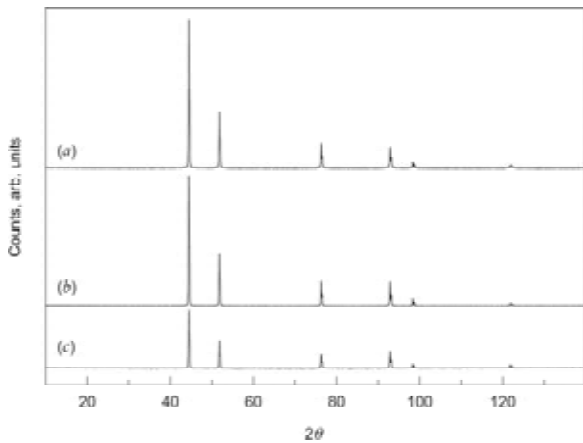
Fig. 5. XRD patterns of (a) carbonyl Ni(cb) and (b) electrolytic Ni(el) nickel powders and (c) foam nickel Ni(f). All XRD patterns are recorded in Cu$K\alpha_{1,2}$ radiation.

structure of an individual extended particle is displayed on the microphotograph obtained at 150000× magnification (Fig. 4c). It is visible that the cobalt particle surface is formed by nanoparticles 20 to 30 nm in size.

The following information was obtained from comparison of the cobalt powders morphology. At the microstructure level, the thermochemical powder Co(th) consists of individual particles and is bimodal. The electrolytic powder Co(el), by contrast, has a dendritic microstructure and is monomodal. At ×10000 magnification, the shape of Co(th) (Fig. 1b) and Co(el) (Fig. 4b) powder particles is similar though the size of the Co(el) particles is almost twice as large as that of the Co(th) particles. At the same time, finer details of the individual particle microstructure are visible, which is why we performed electron microscopy studies of cobalt powders at a greater magnification. Advanced examination of the Co(th) powder microstructure revealed that the smallest size of its particles is 50 to 100 nm. Analogous SEM study of the electrolytic powder Co(el) showed that its large particles of size ~1 mm are formed by well joined 20 to 30 nm nanoparticles. It is therefore clear that the electrolytic powder Co(el) is nanostructured and has a larger interface area than the Co(th) powder obtained by the thermochemical method. In the production of chemical current sources, these morphological differences may provide a certain advantage to the electrolytic powder Co(el).

3.2. Nickel powders and foam

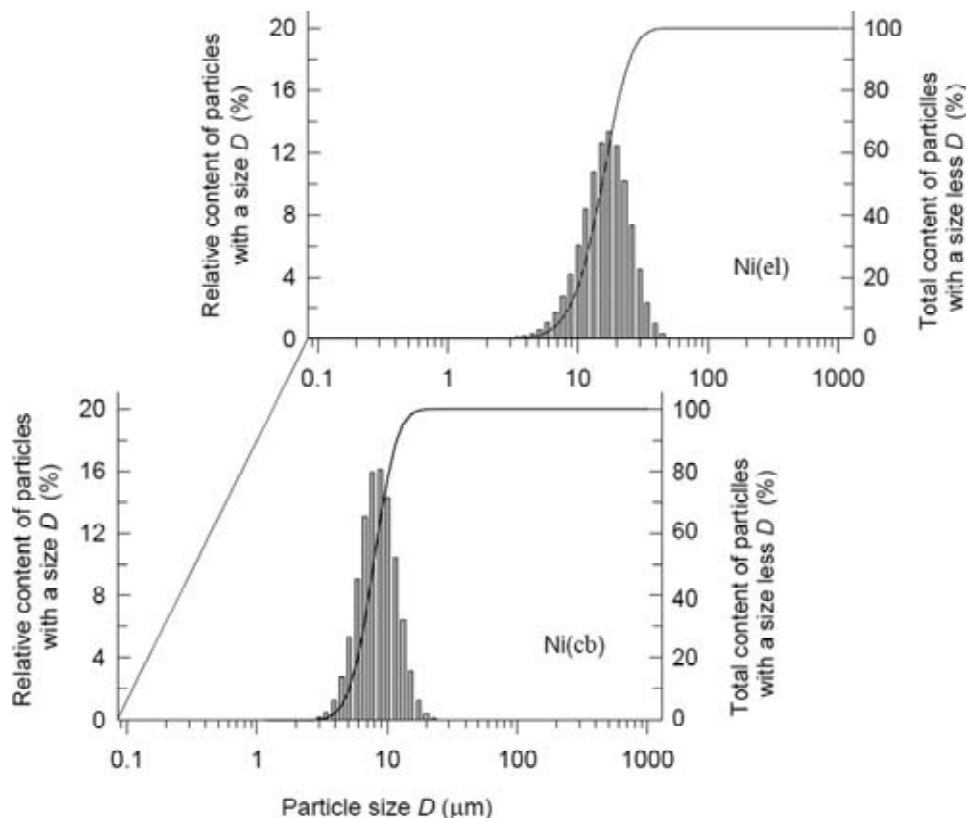The XRD patterns of carbonyl Ni(cb) and electrolytic Ni(el) nickel powders, as well as of foam nickel

Fig. 6. Particle size distributions for the carbonyl Ni(cb) and electrolytic Ni(el) nickel powders.
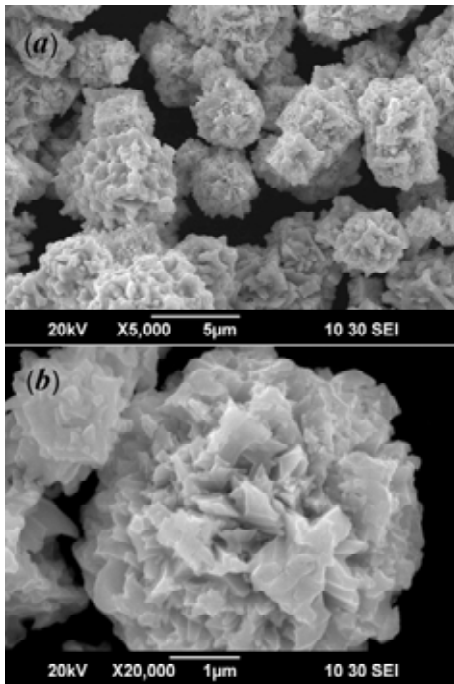
Fig. 7. Scanning electron microscopy of carbonyl nickel powder Ni(cb): (a) 5000× and (b) 20000× magnification.

Ni(f) are depicted in Fig. 5. The both nickel powders and foam nickel are one-phase substances and contain only Ni with a cubic (space group $Fm\overline{3}m$) structure and lattice constant $a = 0.35242\pm0.00002$ nm. The diffraction reflection of the carbonyl powder

Ni(cb) (Fig. 5a) are not virtually broadened, and the average CSR dimension is 210 nm. Thus, the carbonyl powder is not nanocrystalline. According to the data of laser diffraction analysis, the smallest particles in the Ni(cb) powder are ~2 μm in size, half of all the particles are less than 8 μm in size, and 95% of all the particles have a size no more 13 μm (Fig. 6). It means that the particles of carbonyl Ni(cb) powder are agglomerated. This is confirmed by SEM results obtained at different magnifications (Fig. 7): large nickel particles of size 3 to 5 μm, whose shape is close to a distorted cube, have a complicated structure formed by aggregated hedgehog-shaped particles not larger than 1 mm in size. Note that the fractal microstructure of individual nickel particles of size ~0.6 to 0.8 μm, which have a hedgehog shape with 100 to 200 nm long needles, was reported in [8]. A nickel nanopowder was synthesized in study [8] by reduction of $NiCl_2\cdot6H_2O$ with hydrazine sulfate in a strongly alkaline environment.

The diffraction reflections of the electrolytic nickel powder Ni(el) (Fig. 5b) are broadened as compared with those of the carbonyl powder Ni(cb). This broadening of diffraction reflections corresponds to the average size of the CSR of 100 nm.

SEM images of the electrolytic powder Ni(el) (Fig. 8a) demonstrate a coral-like dendritic structure of aggregated particles. At 10000× magnification (Fig. 8b), it is seen that aggregated particles 2 to 3 μm in length and 0.5 to 1.0 μm in width are arranged as
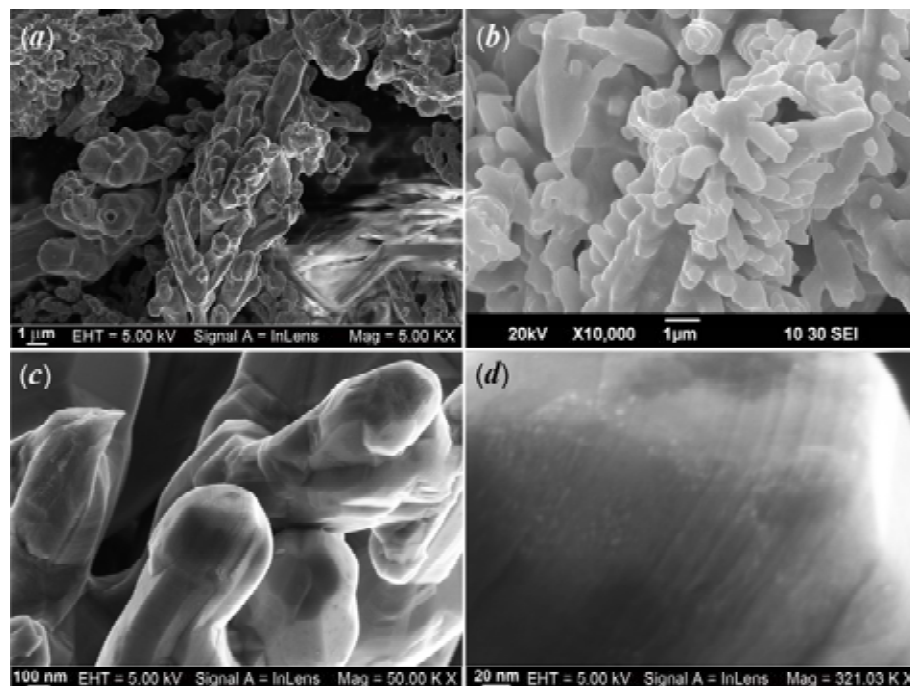

Fig. 8. Scanning electron microscopy of electrolytic nickel powder Ni(el): (a) 5000×, (b) 10000×, (c) 50000×, and (d) 321000× magnification.
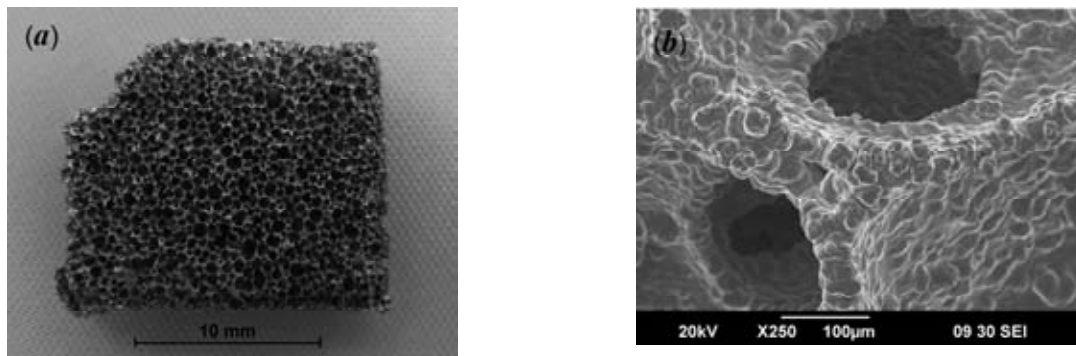
Fig. 9. Optical (a) and scanning electron (b) microscopy of foam nickel Ni(f): the size of pores in foam nickel is 0.2 to 1.0 mm; 50 to 100 μm thick nickel bubble-pore walls are formed by highly aggregated ball-shaped particles 20 to 30 μm in diameter; the porosity of foam nickel is ~96%.

needles on 10 to 15 μm long firtree twigs. In-depth SEM study of the Ni(el) powder at 50000× magnification (Fig. 8c) revealed that the powder contains many particles of ~100 nm in size. This is confirmed by the diffraction reflections broadening on the XRD pattern of electrolytic nickel Ni(el) (Fig. 5b). At 321000× magnification (Fig. 8d), the extended 2 to 3 μm long and ~0.5 μm wide particles are seen to have a layered structure, their surface being formed by 5 to 15 nm nanoparticles.

Study of size distribution of particles of electrolytic Ni(el) powder showed that the smallest particles in the Ni(el) powder are ~3 μm in size, half of all the particles are less than 15 μm in size, average size is equal to 16 μm, and 95% of all the particles have a size no more 28 μm (Fig. 6). Thus, particles of the electrolytic nickel powder Ni(el) are more agglomerated than the particles of Ni(cb) powder.

Fig. 9 displays an optical and SEM images of a foam nickel Ni(f) sample: the pores in foam nickel are 0.2 to 1.0 mm in size and the nickel bubble wall thickness is 50 to 100 μm. The density of foam nickel is ~0.35 g·cm^{-3} and porosity is ~96%. By means of SEM it is seen that the pore walls are formed by tightly aggregated ball-shaped particles 20 to 30 μm in diameter. Foam nickel Ni(f), as judged
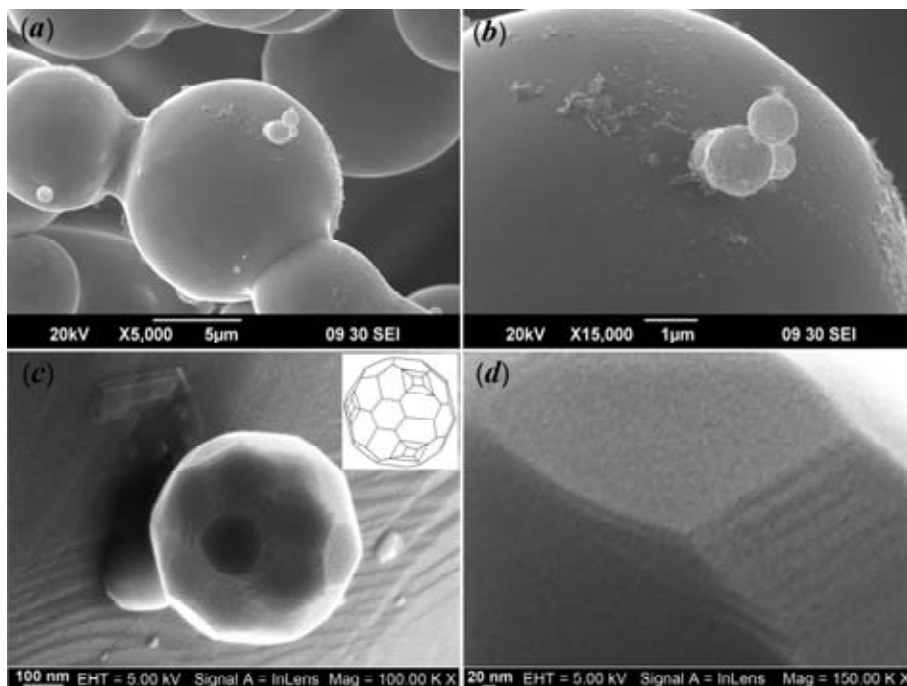

Fig. 10. Scanning electron microscopy of foam nickel Ni(f): (a) 5000×, (b) 15000×, (c) 100000×, and (d) 150000× magnification. The contour of an experimentally observed individual microparticle of foam nickel Ni(f) is shown in the inset in Fig. 10c.
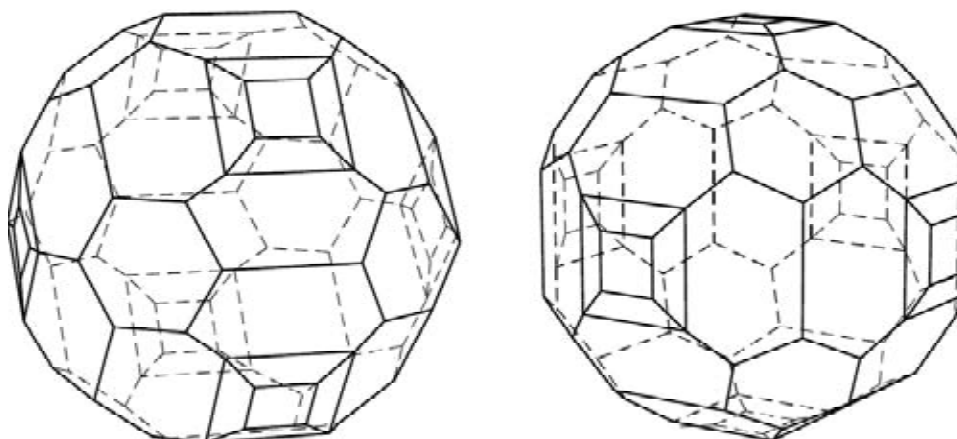
Fig. 11. Two projections of a convex irregular polyhedron modeling the shape of a foam nickel Ni(f) microparticle. The polyhedron has 62 faces (6 regular and 24 irregular tetragons, 8 regular and 24 irregular hexagons), 96 vertexes and 156 edges.
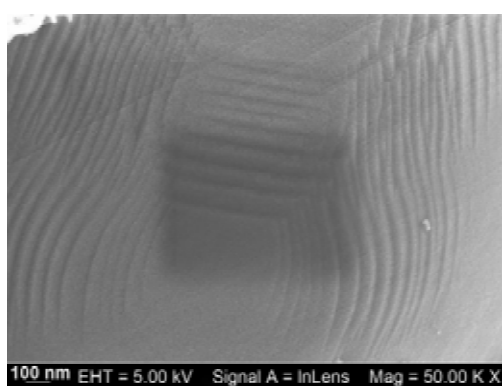

Fig. 12. The layered structure of a foam nickel Ni(f) microparticle with a step-nanoterraced morphology. 50000× magnification.

from its XRD pattern (Fig. 5c), is one-phase and contains only cubic nickel with lattice constant 0.35187 nm. The diffraction reflection broadening corresponds to the average CSR size of 26 nm.

Scanning electron microscopy of foam nickel demonstrates aggregated ball-like particles of size 100 nm to 10 μm, which form a lengthy cage (Figs. 10à and 10b). At ×100000 and ×150000 magnification (Figs. 10c and 10d), individual non-aggregated particles are not of an ideal ball-like shape, but have faceting. This is particularly well seen in the SEM image of an individual ~560 nm-sized microparticle (Fig. 10c), which is a complex-shaped convex polyhedron (Fig. 10c, inset). The shape of a Ni(f) microparticle in the form of an irregular polyhedron with 62 facets (30 tetragons, 8 regular, and 24 irregular hexagons), 96 vertexes, and 156 edges is presented in greater detail in Fig. 11. A regular crystallographic faceting is typical of low-atomic nanoparticles produced by deposition from gaseous phase [12,13,19,20]. The form of facets in the Ni(f) microparticle is distorted considerably and

at the place of large regular tetrahedrons 4-facet pyramids are growing. This is due to destabilization of the regular or semi-regular convex polyhedron shape occurring with an increase in the particle size [12]. The Ni(f) microparticle facets consist of ~10 nm-sized nanoparticles (Fig. 10d), which form 10 to 15 nm thick layers. Successive stacking of layers gives rise to the observed layered structure with a step-nanoterraced morphology (Fig. 12).

Comparison of the nickel powder Ni(el) and foam nickel Ni(f) morphology showed that the Ni(el) powder has a dendritic microstructure, whereas the microstructure of foam nickel is a lengthy cage of ball-shaped particles. At a magnification of 50000 times, the dendrites in the Ni(el) powder are aggregates of microparticles of size ~100 to 200 nm, while the foam nickel cage consists of 100 to 600 nm long microparticles. At maximal magnification from 100000 to 300000 power, it is clear that the Ni(el) powder and foam nickel Ni(f) microparticles are made up of nanoparticles 5 to 15 nm in size which are tightly joined together. Thus, the electrolytic powder Ni(el) and foam nickel Ni(f) are nanostructured.

4. CONCLUSION

In the whole, the morphology and microstructure of particles of the examined nanostructured nickel and cobalt powders can be described with a three-level (according to particle size) model. At the lower level, the powders consist of 50 nm and smaller nanocrystallites, which is confirmed by X-ray diffraction and electron microscopy data. At the next level, the nanocrystallites are united in compact aggregates: extended microparticles of 1 to 2 μm in

length in cobalt powders (Figs. 1b, 4b) and fractal-type microparticles in the electrolytic powder Ni(el) (Figs. 8b, 8c). In cobalt and nickel powders, at the upper level these aggregates are joined into large-size particles and different-shape associates with linear dimensions of 5 to 15 μm or larger (Figs. 1a, 3, 4a, 6, 8a). The same three particle-size levels are observed for the structure of foam nickel Ni(f).

ACKNOWLEDGEMENTS

REFERENCES

[1] S.P. Gubin and Y.A. Koksharov // *Inorg. Mater.* **38** (2002) 1085.

[2] I. Šafařik and M. Šafařikova // *Monatsh. Chem.* **133** (2002) 737.

[3] *Scientific and Clinical Applications of Magnetic Carriers*, ed. by U. Häfeli, W. Schütt, J. Teller and M. Zborowski (Plenum, New York, 1997), p.633.

[4] S.P. Gubin, Y.A. Koksharov, G.B. Khomutov and G.Y. Yurkov // *Uspekhi Khimii* **74** (2005) 539-574, in Russian.

[5] A.I. Gusev // Physics - Uspekhi **41** (1998) 49.

[6] P.S. Liu and K.M. Liang // *Mater. Sci. Techn.* **16** (2000) 575.

[7] Y.N. Lisakov, L.V. Biketova, L.V. Volkov, V.F. Kozyrev, A.S. Mnukhin, Y.M. Pelikh and A.G. Ryabko // Zvetnaya Metallurgiya **11** (2003) 52, in Russian.

[8] Y.A. Zakharov and R.P. Kolmykov // *Polzunovskii Vestnik* **3** (2008) 137, in Russian.

[9] T.A. Schaedler, A.J. Jacobsen, A. Torrents, A.E. Sorensen, J. Lian, J.R. Greer, L. Valdevit and W.B. Carter // *Science* **334** (2011) 962.

[10] W.H. Hall and G.K. Williamson // *Proc. Phys. Soc. London B* **64(11)** (1951) 937.

[11] G.K. Williamson and W.H. Hall // *Acta Metal.* **1** (1953) 22.

[12] A.I. Gusev and A.A. Rempel, *Nanocrystalline Materials* (Cambridge Intern. Sci. Publ., Cambridge, 2004), p.351.

[13] A.I. Gusev, *Nanomaterials, Nanostructures, Nanotechnologies* (Nauka, Moscow, 2nd ed., 2007), p.414, in Russian.

[14] A.S. Kurlov and A.I. Gusev // *Glass Phys. Chem.* **33** (2007) 276.

[15] A. Markström, B. Sundman and K. Frisk // *J. Phase Equil. Diff.* **26** (2005) 152.

[16] A.S. Kurlov, A.I. Gusev and A.A. Rempel // *Intern. J. Refr. Met. Hard Mater.* **29** (2011) 221.

[17] A.S. Kurlov and A.A. Rempel // *Inorganic Materials* **43** (2007) 602.

[18] A.S. Kurlov and A.A. Rempel // *Inorganic Materials* **45** (2009) 380.

[19] M.R. Hoare and P. Pal // *J. Cryst. Growth* **17** (1972) 77.

[20] M.R. Hoare and J. McInnes // *Faraday Discuss. Chem. Soc.* **61** (1976) 12.